CHC22 Clathrin Diverts GLUT4 from the ER-to-Golgi Intermediate Compartment for Intracellular Sequestration

Stéphane M. Camus[1,2,3,4,8], Marine D. Camus[1,2,3,4,8], L. Amanda Sadacca[8] Christopher Esk[5], Gwyn W. Gould[6], Dimitrios Kioumourtzoglou[6,7], Nia J. Bryant[7], Shaeri Mukherjee[3,4*] and Frances M. Brodsky[1,2,3,4,8,*]

[1]Department of Bioengineering and Therapeutic Sciences,
[2]Department of Pharmaceutical Chemistry,
[3]Department of Microbiology and Immunology,
[4]The G.W. Hooper Foundation, University of California San Francisco, San Francisco, CA 94143, USA
[5]IMBA Institute of Molecular Biotechnology GmbH, Vienna, Austria
[6]Institute of Molecular, Cell and Systems Biology, College of Medical, Veterinary and Life Sciences, University of Glasgow, Glasgow, G12 8QQ. UK.
[7]Department of Biology, University of York, York, YO10 5DD. UK
[8]Present address: Division of Biosciences, University College London, London WC1E 6BT, UK
[*]Co-corresponding authors

Running Title: GLUT4 Compartment Formation by CHC22 Clathrin Bypasses the Golgi.

The Glucose Transporter 4 (GLUT4) in muscle and adipose tissue mediates post-prandial blood glucose clearance by insulin-stimulated GLUT4 translocation to the cell surface from an intracellular GLUT4 storage compartment (GSC)[1,2]. Deregulation of this process establishes insulin resistance and contributes to pathogenesis of type-2 diabetes (T2D)[2]. Endocytic pathways targeting GLUT4 to the GSC after insulin-mediated release have been defined extensively in rodent models[3-5]. Here we map the biosynthetic trafficking pathway leading to initial GSC formation, which is less characterised, and differs between humans and rodents. In human muscle and adipocytes, GSC formation involves the non-canonical isoform of clathrin, CHC22, which does not mediate endocytosis and accumulates at sites of GLUT4 sequestration during insulin resistance[6]. Mice have lost the *CLTCL1* gene encoding CHC22[7], and use conventional CHC17 clathrin[3-5] for GSC formation by endocytic pathways that do not replace CHC22 function in human GSC formation[6]. Here we report that CHC22 controls GLUT4 transport from the ER-to-Golgi intermediate compartment (ERGIC) in an unconventional secretory pathway, bypassing the Golgi, to form the human GSC. This specialized route for human GLUT4 membrane traffic has relevance for understanding insulin resistance.

The canonical CHC17 clathrin is formed from three clathrin heavy chains (CHCs) encoded on human chromosome 17, with associated regulatory light chain subunits. CHC17 clathrin is expressed in all tissues and coats vesicles responsible for receptor-mediated endocytosis at the plasma membrane and protein sorting at the *trans*-Golgi network[8]. CHC22 clathrin is formed from

CHCs encoded on human chromosome 22 and exhibits unique biochemical properties and subcellular localization compared to CHC17, indicating a distinct and specific role[6,9]. CHC22 is most highly expressed in muscle cells, though only at 10% of CHC17 levels, and has variable lower expression in other tissues[10]. Depletion of CHC22 from human myotubes and adipocytes abrogates GSC formation and results in loss of insulin-stimulated glucose uptake[6], indicating that CHC22 mediates pathways to GSC formation that are not replaced by CHC17. Transgenic expression of CHC22 in mouse muscle, which normally expresses only CHC17 clathrin, was found to disrupt GLUT4 trafficking, resulting in expansion of the GSC and over-sequestration of GLUT4 leading to high blood glucose[6]. Although CHC22 interacts with some adaptor molecules that recruit CHC17 to membranes[6,9] and is required for a retrograde transport pathway from endosomes[10], which has been shown to be important in murine GSC formation[11], our studies to date indicate that CHC22 must play a role in human GSC formation that is distinct from the role of CHC17 in murine GSC formation.

To further define the role of CHC22 in formation of the human GSC, we developed a model system in which GLUT4 translocation can be easily studied. This was necessitated by limited experimental capacity of available human muscle and adipocyte cell lines and the widely acknowledged problem of detecting endogenous GLUT4 at the cell surface. We produced a stable HeLa cell transfectant (HeLa-GLUT4) expressing human GLUT4 containing a haemagglutinin (HA) tag in the first exofacial loop and a GFP tag at the intracellular carboxyl terminus, a construct that has been extensively

characterized and validated for the study of intracellular GLUT4 trafficking in rodent cells[12,13]. HeLa cells were chosen because they have levels of CHC22 comparable to those in human muscle cells[10] and they also express sortilin, another protein important for formation of the GSC[14,15,16]. GLUT4 was sequestered intracellularly in HeLa-GLUT4 cells in the absence of insulin (basal), localized to both peripheral vesicles (arrowheads) and a perinuclear depot (arrows), reminiscent of insulin-releasable vesicles and the vesiculo-tubular GSC of murine cells, respectively[3,17] (Fig. 1a). Perinuclear GLUT4 co-localized with the GSC marker syntaxin-6 (STX-6) and with CHC22 (Fig. 1b). After 15 minutes of insulin treatment, GLUT4 was detected at the cell surface with a monoclonal antibody to the HA tag (anti-HA) (Fig. 1a). Additionally, insulin exposure induced phosphorylation of AKT and its substrate AS160, two modifications required for insulin-stimulated GLUT4 translocation[2] (Fig. 1c). Insulin-mediated GLUT4 translocation in the HeLa-GLUT4 cells was quantifiable using a fluorescence activated cell sorter (FACS) to measure the mean fluorescence intensity of surface GLUT4 relative to the total GFP-GLUT4. GLUT4 expression at the plasma membrane increased 2-fold after 15 minutes of insulin treatment (Fig. 1d).

In rodent models (3T3-L1 mouse adipocytes and L6 rat myotubes), GLUT4 released by insulin to the plasma membrane can return by endocytosis to the GSC within 30 minutes[17,18]. Replicating this analysis in the HeLa-GLUT4 model, we labelled surface GLUT4 with anti-HA antibody following insulin stimulation and observed that internalised GLUT4 accessed a perinuclear compartment overlapping with STX-6 with similar kinetics (Supplementary Fig.

1a, b). Internalised GLUT4 overlapped to the same extent with CHC22 (Fig. 1e, f) after 10 and 30 minutes of re-uptake. The GSC formed in the HeLa-GLUT4 cells also had properties of the human GSC, in that siRNA-mediated depletion of CHC22 induced dispersion of the GSC and inhibited insulin-stimulated GLUT4 translocation (Fig. 1g, h), as previously observed for human muscle cells[10]. Taken together, our results show that HeLa cells stably expressing HA-GLUT4-GFP depend on CHC22 for GLUT4 sequestration and form an insulin-sensitive GSC, which is accessed by GLUT4 recaptured from the cell surface. Thus, the model recapitulates features of the GSC observed for both mouse and human cells and can be used for analysis of pathways involved in GLUT4 trafficking in human cells. We note that during the course of this work, other laboratories developed and validated similar models of insulin-dependent GLUT4 translocation in HeLa cells[19,20].

Our previous studies identified a function for CHC22 in retrograde transport from endosomes, but only limited overlap between CHC22 and the endosomal marker Rab 9 was observed[10]. Suspecting that CHC22 might operate in an additional pathway leading to GSC formation, we analysed both the HeLa-GLUT4 cells and differentiated human myotubes (LHCNM2) for overlap between CHC22 and markers of the secretory pathway, as the biosynthetic origins of the GSC are not fully characterised. For this study, we used a new polyclonal antibody specific for CHC22 and not reactive with CHC17 that had stronger activity in immunofluorescence staining than our previously produced anti-CHC22 antibodies[10, 21]. In both HeLa-GLUT4 and differentiated LHCNM2 cells, we observed significant co-localization of

CHC22 and two markers of the ER-to-Golgi Intermediate Compartment (ERGIC), namely p115 and ERGIC-53 (Fig. 2a-d), while there was no significant co-localization of CHC22 with endoplasmic reticulum (ER) markers β-COP and calreticulin (Supplementary Fig. 2a-c) in either cell type. GLUT4 internalised after insulin stimulation also showed time-dependent co-localization with ERGIC-53, indicating that the GSC, where recaptured GLUT4 accumulates, is closely associated with the ERGIC (Supplementary Fig. 2d, e).

For both HeLa-GLUT4 and LHCNM2 cells, intermediate levels of co-localization were observed between CHC22 and markers of the *trans*-Golgi network (TGN46) or the *cis*-Golgi (GM130) (Supplementary Fig. 2f-i). Considered together, these data are consistent with previous mapping of CHC22 activity to retrograde transport from late endosomes[10], and suggest a further role for CHC22 possibly at the ERGIC or the *cis*-Golgi. To map CHC22 relative to these compartments of the secretory pathway and the GSC, we treated HeLa-GLUT4 and LHCNM2 myotubes with Brefeldin A (BFA) (Supplementary Fig. 3a, 3b). We previously showed that BFA does not cause CHC22 to dissociate from intracellular membranes[9] and others have shown that the GSC is not affected by BFA[22]. After BFA treatment of either cell type, CHC22 co-distributed with the ERGIC marker p115 and segregated away from the persisting GSC, confirming the BFA-resistance of the GSC and supporting the association of CHC22 with ERGIC membrane. This result further suggests that CHC22 is not a final component of the stable GSC, although involved in GSC formation[6].

To establish whether CHC22 has functional activity where it localizes with ERGIC markers, we tested whether CHC22 plays a role in the life-cycle of the facultative intracellular pathogen *Legionella pneumophila* (*Lp*), which hijacks membrane from the early secretory pathway to create an *Lp*-containing vacuole (LCV), in which it can replicate. Upon infection, *Lp* secretes ~300 effector proteins, through a type IV secretion system, some of which enable recruitment of ER proteins Sec22b, Rab1 and Arf1 to the LCV[23], which are needed for its formation. The mature LCV retains ER-like properties, including the lumenal proteins calnexin, BiP and calreticulin and does not acquire Golgi markers[23-25]. Given that the LCV is derived from the ER, and that CHC22 localizes to a pathway emerging from the ER, we tested whether CHC22 associates with membranes involved in LCV formation by transient expression of GFP-tagged CHC22 or GFP-tagged CHC17 in A549 human lung adenocarcinoma cells prior to *Lp* infection. CHC22, but not CHC17, was associated with the membranes surrounding the LCV (Fig. 3a, b). CHC22 did not localize with the isogenic avirulent *Lp* mutant Δ*dotA,* which enters cells but lacks a functional secretion system and cannot deploy effectors to induce a replication-supportive vacuole (Fig. 3a, b).

To address whether CHC22 is involved in transfer of membrane to the LCV, we treated A549 cells with siRNA targeting CHC22 prior to infection. The resulting CHC22 down-regulation significantly compromised recruitment of Sec22b to the bacterial vacuole at 1 hour post-infection (Fig. 3c, d), suggesting defective vacuole maturation. This was confirmed by assessing bacterial replication eight hours after infection with WT or ΔdotA *Lp* strains

following CHC22 or CHC17 silencing. CHC22 silencing reduced the proportion of vacuoles containing >4 *Lp* by more than 9-fold, while CHC17 silencing reduced vacuoles with >4 *Lp* by approximately 2-fold (Fig. 3e), suggesting a need for CHC22 to form a replicative vacuole and a possible role for CHC17 during bacterial uptake. The latter conclusion is supported by the observation that CHC22 down-regulation increased the percentage of vacuoles with 1 *Lp*, showing that bacterial entry was still occurring, but vacuoles with 1 *Lp* comprised a smaller percentage in cells silenced for CHC17 infected with an equivalent number of bacteria. Infection of cells transfected with siRNA targeting CHC22 with an equivalent number of avirulent ΔdotA *Lp* showed that these bacteria could also enter cells, with 94% vacuoles observed harbouring only 1 *Lp* (Fig. 3e). Together these data suggest that *Lp* hijacks CHC22 to acquire host early secretory membrane needed for maturation of a replication-competent LCV, and that *Lp* effectors might interact with CHC22 or its partners. We did not see recruitment of GLUT4 to the LCV (Supplementary Fig. 4a, b), indicating that the bacteria-induced pathway does not contain all the components needed for formation of a GSC. However, these data suggest CHC22 has an active role in membrane traffic emerging from the ER.

A previous study tracking transiently expressed GFP-tagged GLUT4 suggested that, in 3T3-L1 adipocytes, newly synthesized GLUT4 accesses the GSC from the secretory pathway, before reaching the plasma membrane[26]. Based on CHC22 localization and its role in membrane transport from the early secretory pathway during LCV maturation, we

hypothesized that, in humans, CHC22 controls GSC formation from the secretory pathway directly from the ERGIC. The potential existence of this pathway was supported by the earlier demonstration that overexpression of a dominant negative fragment of p115 abrogated the GLUT4 insulin response in 3T3-L1 cells[27]. To investigate the involvement of secretory pathways in GSC formation, we depleted p115, CHC22, CHC17 and GM130 from HeLa-GLUT4 cells using siRNA (Fig. 4a), assessed the morphology of the GSC by microscopy (Fig. 4b, c) and evaluated the impact on insulin-induced GLUT4 translocation by FACS (Fig. 4d). Silencing of p115 or of CHC22 abrogated or reduced perinuclear localization of GLUT4 and increased GLUT4 dispersion in the cell periphery, with down-regulation of each affecting the distribution of the other (Fig. 4b). Insulin-stimulated GLUT4 translocation was lost from cells silenced for p115 or CHC22 (Fig. 4d), while CHC17 silencing had a partial effect on GLUT4 translocation (Fig. 4d), consistent with previous observations for CHC22 and CHC17 down-regulation[6]. Notably, however, siRNA-mediated down-regulation of the *cis*-Golgi protein GM130, functionally confirmed by reduction of alkaline phosphatase secretion[28] (Fig. 4e), did not abrogate insulin-stimulated GLUT4 translocation (Fig. 4d) or affect the distribution of perinuclear GLUT4 (Fig. 4c). These results suggest p115 and CHC22 participate in a step of GSC formation that diverts GLUT4 from the ERGIC and bypasses transport through the Golgi.

For another indication of how formation of the GSC depends on CHC22 and p115, these proteins and CHC17 were depleted by siRNA (Supplementary Fig. 5a-c) and levels of GSC-associated proteins, including insulin-regulated

amino peptidase (IRAP), sortilin[14] and Golgi-localized γ ear-containing ARF-binding protein 2 (GGA2)[15,26,29], were assessed by quantitative immunoblotting (Fig. 5a-c). Analysis of statistically significant changes indicated that CHC22 depletion but not CHC17 depletion reduced cellular levels of GLUT4, sortilin, and GGA2. Depletion of p115 strongly reduced IRAP levels. Depletion of CHC17 increased CHC22, as previously observed[6,10] and also slightly increased GGA2 levels. The differential effects of p115, CHC22 and CHC17 depletion suggest that each of these membrane traffic mediators contribute differently to GSC formation. A biochemical association between p115 and IRAP has already been established[27] and their association occurs whether or not cells have a GSC, as IRAP has a wider cellular expression pattern than GLUT4[30]. Based on the demonstration of lumenal interactions between sortilin and IRAP, sortilin and GLUT4[15] and IRAP and GLUT4[30], it has been proposed that IRAP, which initially traffics with p115[27], becomes associated with sortilin and GLUT4 during the formation of the GSC[30], at which point the GSC becomes segregated from the constitutive secretory pathway. Sortilin is known to recruit the GGA2 adaptor[31], which has been previously implicated in GLUT4 traffic to the GSC[16,26,29] and preferentially binds to CHC22 over CHC17[6]. Thus, CHC22 could be recruited as a membrane coat that coalesces the players for GSC formation and stabilises their interaction for forming a specialised compartment. Our data on CHC22 localization presented here suggests that the process of initial sorting to the GSC, triggered by the meeting of the p115-IRAP complex with GLUT4 and sortilin, occurs at the ERGIC (Fig 5d), which is consistent with previous studies suggesting direct GLUT4 diversion from the secretory pathway to the

GSC[26] in a p115-dependent step[27]. Interestingly, p115 is not recruited to the *Lp* early replicative vacuole[23] and it has been proposed that one of *Lp*'s secreted effectors can functionally replace p115 to facilitate recruitment of vesicles from the early secretory pathway. CHC22 may also be recruited by the bacterial effector, while GLUT4 apparently is not. The differential dependence of GLUT4 and alkaline phosphatase (and other proteins[32,33]) on p115 for export suggests the ERGIC is a sorting station for several secretory pathways, some of which, such as autophagy[34], bypass conventional secretion.

Our proposed pathway of GSC formation from the ERGIC (Fig. 5d) is consistent with earlier analysis of GLUT4 glycosylation. The rate that the carbohydrate side chains on newly synthesized GLUT4 become resistant to cleavage by Endoglycosidase H was shown to be considerably delayed (3 days vs 1 hour) compared to that of GLUT1, which is constitutively expressed on the cell surface[35,36]. This could be explained by direct GLUT4 diversion to the GSC from the ERGIC, followed by a process of carbohydrate maturation that depends on secretion and recapture through a retrograde recycling compartment[17] with low-level access to enzymes of the medial and *trans*-Golgi. Our model is also consistent with the reported ERGIC localization of the TUG protein involved in GLUT4 vesicle retention[37] and potentially with the recent discovery of Sec16A as a target for Rab10 activity[38]. Sec16A seems to participate in GLUT4 membrane traffic independently of its conventional COPII partners[38]. Its presence at ER exit sites and documented interaction

with p115[39] suggests that Sec16A could be sequestered from the ERGIC during the pathway of GSC formation suggested here.

We propose that for both humans and mice, GSC formation is initiated by direct diversion from the ERGIC to sequester GLUT4 away from the conventional secretory pathway in a step that involves p115 and IRAP. Then, once GLUT4 is released by insulin to the cell surface, it is returned to the GSC by retrograde transport from the endosome-TGN recycling pathway, which can expose GLUT4 to carbohydrate modification. The difference between human and murine GLUT4 traffic is that humans have CHC22 clathrin, which can localize to the ERGIC and thereby capture GGA2-bound sortilin-IRAP-GLUT4 complexes as they coalesce in the ERGIC to enhance GLUT4 delivery to the GSC (Fig. 5d). Thus the murine pathway is likely to be more dependent on the recapture and recycling from the plasma membrane to keep the GSC replenished, while humans have a more robust route to their GSC from the ERGIC. For both murine and human cells, CHC17 clathrin is needed for GLUT4 endocytosis from the plasma membrane and, in murine cells, CHC17 is the likely mediator of the retrograde endosome-TGN recycling pathway that involves AP1[40] and GGA2[41]. Our previous studies of CHC22 suggested it also functions in this recycling pathway because CHC22 depletion affected mannose-6-phosphate receptor (M6PR) traffic[10], which depends on retrograde transport. However, our demonstration here that CHC22 depletion reduces cellular levels of GGA2 could also account for effects on the M6PR pathway[41,42] so it is not clear if CHC22 plays this second role in human GLUT4 transport in addition to its role in GSC formation from

the ERGIC. CHC17 does not localize to the ERGIC and it cannot replace CHC22 function in human GSC formation, indicating that human cells depend more heavily on the ERGIC-derived pathway and cannot maintain a GSC with only the CHC17-dependent endocytosis and recycling pathway, as occurs in murine cells. We reiterate here that CHC22, at endogenous levels of expression, does not have a role in receptor-mediated endocytosis from the plasma membrane[9,10].

The evolutionary retention of CHC22 in humans, following the gene duplication process that generated it, may have been advantageous for tighter control of GLUT4 sequestration in order to maintain high levels of blood glucose for large brain function during starvation. Loss of CHC22 in mice may have been favoured by a need to regularly clear blood glucose generated by a nibbling diet (and no need to feed a large brain). Thus, the extra role of CHC22 in human GSC formation may provide too much GLUT4 sequestration as we transition to a nibbling diet. Insulin resistance is sensitive to levels of available GLUT4[43], so by accumulating on the expanded GSC, which occurs as a result[6], CHC22 could potentially exacerbate human insulin resistance.

Figure Legends

Figure 1: HeLa-GLUT4 cells form an insulin-sensitive perinuclear GLUT4 storage compartment dependent on CHC22 clathrin.

(**a**) Representative images of GLUT4 (exofacial HA-tag, internal GFP tag) in HeLa-GLUT4 cells before (basal) or after insulin treatment. GLUT4 at the plasma membrane was detected by immunofluorescence (IF) following surface labelling with anti-HA monoclonal antibody (red). Total GLUT4 (green) was detected by GFP tag. Arrows show the GLUT4 storage compartment. Arrowheads point to peripheral vesicles. Scale bars: 7.5 μm. (**b**) Representative IF staining for syntaxin-6 (STX-6, red) and CHC22 (blue) in HeLa-GLUT4 cells with GLUT4 detected by GFP tag (green). Scale bars: 5 μm. (**c**) Representative immunoblot for phospho-AKT (p-AKT), phospho-AS160 (p-AS160), total AS160 and β-actin in HeLa-GLUT4 cells before (basal) and after insulin treatment. The migration position of molecular weight (MW) markers is indicated at the left in kilodaltons (kDa). (**d**) Left panel – Representative FACS histogram of surface GLUT4 fluorescence intensities (signal from anti-HA labelling) before (basal) and after insulin treatment; Right panel – quantification of surface:total GLUT4 (HA/GFP mean fluorescence intensity signals). Data expressed as mean ± SEM, N=3, 10,000 cells acquired per experiment. Two-tailed Student's t-test with equal variances: **$p<0.01$. (**e**) Representative IF staining for CHC22 (red) and internalised surface HA-tag (blue) of HeLa-G4 cells at 0, 10 or 30 minutes after insulin treatment. GLUT4 is detected by GFP tag (green). Scale bars: 5 μm. (**f**) Pearson's overlap quantification between CHC22 and HA-tag. Data expressed as mean ± SEM, N=3**,** 11-26 cells per experiment as represented

in (e). One-way ANOVA $p<0.0001$, Bonferroni's multiple comparison post-hoc test *$p<0.01$; ****$p<0.0001$. (**g**) Representative IF staining for CHC17 (red) and CHC22 (blue) in HeLa-GLUT4 cells transfected with control siRNA (non-targeting) or siRNA targeting CHC17 (siCHC17) or CHC22 (siCHC22), with GLUT4 detected by GFP tag (green). Arrows point to CHC22-depleted cell. Scale bars: 10 µm for siControl and siCHC17 and 7.5 µm for siCHC22. (**h**) Representative FACS histogram of surface GLUT4 fluorescence intensity (signal from anti-HA labelling) in HeLa-GLUT4 cells transfected with control siRNA or siRNA targeting CHC22 (siCHC22) before (basal) or after treatment with insulin. Histograms are extracted from experiment quantified in Fig. 4d. Merged images in (a), (b), (e), (g) show red/green overlap in yellow, red/blue overlap in magenta, green/blue overlap in turquoise, and red/green/blue overlap in white.

Figure 2: CHC22 localises to the ER-to-Golgi Intermediate Compartment (ERGIC). Representative immunofluorescence staining for CHC22 (blue) and ERGIC markers, p115 (red) or ERGIC-53 (red), in (**a**) HeLa-GLUT4 cells and (**c**) human LHCNM2 myotubes. GLUT4 (green) was detected by IF of endogenous protein in LHCNM2 cells and by GFP tag in HeLa-GLUT4 cells. Scale bars: 5 and 7.5 µm for (a) and (c), respectively. Pearson's overlap quantification between CHC22 and ERGIC markers p115 and ERGIC-53 in (**b**) HeLa-GLUT4 and in (**d**) human LHCNM2 myotubes. Data expressed as mean ± SEM, N=3, 4-10 cells across 3 independent samples, as represented in (a) and (c). Values above the red line (set at 0.3) indicate overlap. Merged images in (a) and (c) show red/green overlap in yellow, red/blue overlap in

magenta, green/ blue overlap in turquoise, and red/green/blue overlap in white.

Figure 3: CHC22 associates with *Legionella pneumophila* vacuole and is needed for formation of a vacuole that supports bacterial replication.

(**a**) Representative images of *Legionella pneumophila* (*Lp*)-infected A549 cells transiently transfected with GFP-tagged CHC22 or CHC17 (green). One hour after infection with either wild type (WT) or mutant ΔdotA *Lp* (MOI=50), bacteria were detected by immunofluorescence (IF, red). Arrows point to *Lp* and boxed inserts (upper right or left) show Lp region at 5X magnification. Scale bars: 10 µm, referring to main image. (**b**) Quantification of the proportion of *Lp* vacuoles (1h post-infection) positive for CHC22 or CHC17. Data expressed as mean ± SEM, N=3, 4 to 35 vacuoles counted per experiment performed as represented in (a). One-way analysis of variance (ANOVA) $p<0.0001$, Bonferroni's multiple comparison post-hoc test ***$p<0.001$. (**c**) Representative IF images of single A549 cells from cultures treated with siRNA targeting CHC22 or with control (non-targeting) siRNA and labelled for Sec22b (red) and CHC22 (green), 1h post-infection with wild-type *Lp* (MOI=50). Arrows point to *Lp* detected with DAPI. Boxed inserts (upper or lower left) show Lp region at 5X and 2X magnification for siControl and siCHC22, respectively. Scale bar: 5 µm referring to main images. (**d**) Quantification of the proportion of *Lp* vacuoles staining positive for Sec22b. Data expressed as mean ± SEM, N=4, 10 to 20 vacuoles counted per experiment as represented in (c). Two-tailed Student's t-test with equal variances: ***$p<0.001$ (**e**) Quantification of the proportion of replicative

vacuoles (8 hours post-infection) containing 1, 2 to 4, or more than 4 WT *Lp* or ΔdotA *Lp* after treatment with siRNA targeting CHC22 or CHC17 or control siRNA (Data expressed as mean ± SEM, N=3, over 140 vacuoles counted per experiment). One-Way ANOVA $p<0.0001$, followed by Bonferroni's multiple comparison post-hoc test was performed to compare the number of cells with a vacuole containing more than 4 bacteria. ****$p<0.0001$ versus siControl-transfected cells infected with WT *Lp*. ++++$p<0.0001$ versus siControl-transfected cells infected with ΔdotA *Lp*. Merged images in (a) and (c) show red/green overlap in yellow, red/blue overlap in magenta, green/ blue overlap in turquoise, and red/green/blue overlap in white.

Figure 4: Targeting GLUT4 to the perinuclear GLUT4 Storage Compartment is affected by depletion of p115 and CHC22 from the ER-to-Golgi Intermediate Compartment but not disruption of the Golgi by GM130 depletion**.** (**a**) Immunoblotting for CHC22, CHC17, p115 GM130 and β-actin after treatment of HeLa-G4 cells with siRNA targeting CHC17 or CHC22 or with control (non-targeting) siRNA. The migration position of molecular weight (MW) markers is indicated at the left in kilodaltons (kDa). (**b**) Representative immunofluorescence (IF) staining for CHC22 (red) and p115 (blue) in HeLa-GLUT4 cells after treatment with siRNAs as in (a), with GLUT4 detected by GFP tag (green). N, nucleus. Arrows point to CHC22-depleted cell. Scale bars: 10 μm. (**c**) Representative IF staining for GM130 (yellow), p115 (red) and CHC22 (blue) in HeLa-GLUT4 cells after treatment with siRNA targeting GM130 or with control siRNA, with GLUT4 detected by GFP tag (green). Scale bars: 25 μm. (**d**) Quantification by FACS, as in Fig. 1d, of surface:total

GLUT4 in HeLa-G4 cells treated with siRNA targeting CHC22, CHC17, p115 or GM130 or with control siRNA with (+) or without (-) exposure to insulin. Data expressed as mean ± SEM, N=9, 10,000 cells acquired per experiment. One-way ANOVA $p<0.0001$, followed by Bonferroni's multiple comparison post-hoc test ****$p<0.0001$; ***$p<0.001$; **$p<0.01$ versus untreated (-). (**e**) Quantification of alkaline phosphatase secretion index for HeLa-G4 cells treated with siRNA targeting CHC22, CHC17, p115 or GM130 or with control siRNA. The alkaline phosphatase secretion index is the ratio of secreted enzyme activity (culture medium) to total cellular activity (secreted plus cell lysate). Data expressed as mean ± SEM, N=13-19 independent samples across 2 independent assays. One-way ANOVA $p<0.0001$, followed by Bonferroni's multiple comparison post-hoc test **$p<0.01$ versus siControl. Merged images in (b) and (c) show red/green overlap in yellow, red/blue overlap in magenta, green/ blue overlap in turquoise, and red/green/blue overlap in white.

Figure 5: Downregulation of p115, CHC22 and CHC17 indicates they play distinct roles in GLUT4 membrane traffic.

(**a-c**) Levels of proteins involved in GLUT4 membrane traffic were detected by quantitative immunoblotting following siRNA-treatment of HeLa-GLUT4 cells to deplete (a) CHC22, (b) p115 or (c) CHC17. Cells were transfected with targeting siRNA or with control (non-targeting) siRNA (40 nM for 72h) and cell lysates were immunoblotted for CHC22, CHC17, p115, IRAP, GLUT4, sortilin, GGA2 and β-actin. Blot signals were normalised to β-actin for each experiment and the fold change (negative value indicates decrease and

positive indicates increase) relative to the normalised signal in control-treated cell lysates is plotted. Representative blots are shown in Supplementary Fig. 5. Data expressed as mean ± SEM, N=7-8. Two-tailed Student's t-test, with Welch's correction where variances were unequal: *p<0.05; **p<0.01; ***p<0.001. (**d**) Model of CHC22's role in human GLUT4 trafficking to the GLUT4 storage compartment (GSC). Newly synthesized GLUT4, IRAP and sortilin traffic from the endoplasmic reticulum to the ER-to-Golgi Intermediate Compartment (ERGIC), with IRAP bound to p115. At the ERGIC, a complex forms between sortilin, IRAP-p115 and GLUT4 that recruits GGA2 via sortilin and potentially by ubiquitination of GLUT4[40]. The GGA2 binding promotes sequestration in a CHC22 clathrin coat at the ERGIC, which sorts GLUT4, IRAP and sortilin directly to the GSC. GLUT4 and IRAP then leave the GSC in vesicles that can translocate to the plasma membrane in response to insulin. After plasma membrane translocation, GLUT4 undergoes CHC17 clathrin-dependent endocytosis, and is recycled back to the GSC via the retrograde pathway from late endosomes to the TGN, which could involve CHC22, CHC17 or both clathrins.

SUPPLEMENTARY INFORMATION

Figure S1: Surface GLUT4 can traffic to the GLUT4 storage compartment in HeLa-GLUT4 cells.

(**a**) Representative immunofluorescence (IF) staining for internalised surface-labelled GLUT4 (HA-tag, blue) and syntaxin 6 (STX-6, red) for HeLa-GLUT4 cells at 0, 10 or 30 minutes after insulin treatment. Total GLUT4 is detected by GFP tag (green). Scale bars: 7.5 µm. Merged images show red/green

overlap in yellow, red/blue overlap in magenta, green/ blue overlap in turquoise, and red/green/blue overlap in white. (**b**) Pearson's overlap quantification for labelling of STX-6 and HA-tag (Data expressed as mean ± SEM, N=3**,** 14-19 cells per experiment). One-way analysis of variance (ANOVA) $p<0.0001$, Bonferroni's multiple comparison post-hoc test ****$p<0.0001$.

Figure S2: Localisation of CHC22 and GLUT4 relative to markers of the secretory pathway in HeLa-GLUT4 and LHCNM2 human myotubes.

(**a**) Representative immunofluorescence (IF) staining for CHC22 (red or blue), β-COP (blue) and calreticulin (red) in HeLa-GLUT4 cells. Scale bars: 5 µm. (**b**) Quantification of Pearson's overlap coefficient for experiments represented in (a). Data expressed as mean ± SEM, 13 to 14 cells across 3 independent samples were analysed. (**c**) Representative IF staining for CHC22 (blue), calreticulin (red) and endogenous GLUT4 (green) in LHCNM2 myotubes. Scale bars: 30 µm. (**d**) Representative IF staining for internalised surface-labelled GLUT4 (HA-tag, blue) and ERGIC-53 (red) for HeLa-G4 cells after 0, 10 or 30 minutes of insulin treatment. Total GLUT4 is detected by GFP tag (green). Scale bars: 30 µm. (**e**) Pearson's overlap quantification for labelling of ERGIC-53 and HA-tag, Data expressed as mean ± SEM, 6-14 cells across 3 independent samples were analysed). One-way ANOVA $p<0.0001$, Bonferroni's multiple comparison post-hoc test ****$p<0.0001$. (**f**) Representative IF staining for CHC22 (blue), GM130 (red) and TGN46 (red) in HeLa-GLUT4 cells. Scale bars: 5 µm. (**g**) Quantification of Pearson's overlap coefficient for experiments represented in (f). Data expressed as mean ± SEM,

2-7 cells across 3 independent samples were analysed. (**h**) Representative IF staining for GM130 (green), TGN46 (green), p115 (red) and CHC22 (blue) in LHCNM2 myotubes. Scale bars: 7.5 µm. (**i**) Quantification of Pearson's overlap coefficient for experiments represented in (h). Data expressed as mean ± SEM, 19-20 cells across 3 independent samples were analysed. For panels (a), (d) and (f) GLUT4 is detected by GFP signal (green). Merged images in (a), (c), (d), (f) and (h) show red/green overlap in yellow, red/blue overlap in magenta, green/ blue overlap in turquoise, and red/green/blue overlap in white. For Pearson's overlap quantification, values above the red line (set at 0.3) indicate overlap.

Figure S3: CHC22 distributes with p115 following Brefeldin A treatment. Representative immunofluorescence (IF) staining for CHC22 (blue) and p115 (red) in (**a**) HeLa-GLUT4 cells or (**b**) LHCNM2 myotubes treated or not with Brefeldin A (BFA). GLUT4 (green) was detected by GFP tag in HeLa-G4 cells and by IF of endogenous protein in LHCNM2 cells. Scale bars: 5 and 25 µm for (a) and (b), respectively. Merged images in (a) and (b) show red/green overlap in yellow, red/blue overlap in magenta, green/ blue overlap in turquoise, and red/green/blue overlap in white.

Figure S4: GLUT4 is not recruited to *Legionella pneumophila*'s replicative vacuole. (**a**) Representative images of A549 cells transiently transfected with HA-GLUT4-GFP (green), infected with wild type *Legionella pneumophila* expressing mono-DsRed protein (Lp-DsRed, MOI=50, red) and labelled (blue) 1 hour post-infection with antibodies against CHC17 (upper panel) or CHC22

(lower panel). Merged images show red/green overlap in yellow, red/blue overlap in magenta, green/blue overlap in turquoise, and red/green/blue overlap in white. Scale bars: 5 µm. (**b**) Quantification of the proportion of bacterial vacuoles positive for HA-GLUT4-GFP. Data expressed as mean ± SEM, N=2, 8 and 13 vacuoles counted per experiment).

Figure S5: Differential reduction of proteins involved in GLUT4 membrane traffic following depletion of p115, CHC22 or CHC17 by siRNA treatment.

(**a, b**) Representative immunoblots of HeLa-GLUT4 cells transfected with siRNA targeting CHC22, CHC17 or p115 or with control siRNA showing levels of CHC22, GLUT4, GGA2, CHC17, p115, Sortilin and β-actin. (**c**) Representative immunoblots of HeLa-GLUT4 cells transfected with siRNA targeting CHC22, CHC17 or p115 or with control siRNA showing levels of IRAP and β-actin. The migration position of molecular weight (MW) markers is indicated at the left in kilodaltons (kDa) in (a-c).

Funding sources:

Postdoctoral fellowship from the American Heart Association to SMC.

National Institutes of Health, USA (NIH) R01 DK095663 to FMB and NIH R01 AI118974 to SM.

NJB and GWG were supported by grants from Diabetes UK, ref 13/0004725 and 11/0004289.

Acknowledgements:

The authors thank Sean Treacy-Abarca for technical support, Dr Timothy McGraw for the plasmid encoding HA-hGLUT4-GFP, Dr Craig Roy for the monoclonal antibody against p115 and the polyclonal antibody against *Legionella pneumophila*.

Authors Contribution:

SMC, SM and FMB conceived and designed the experiments.

SMC, MDC performed the experiments.

SMC, MDC, SM and FMB analysed the data.

CE, DK, GWG, and NJB contributed reagents/materials/analysis tools.

SMC, MDC, LAS and FMB wrote the paper with input from SM, GWG and NJB.

1. Leto, D. & Saltiel, A.R. Regulation of glucose transport by insulin: traffic control of GLUT4. *Nat Rev Mol Cell Biol* **13**, 383-396 (2012).
2. Bogan, J.S. Regulation of glucose transporter translocation in health and diabetes. *Annu Rev Biochem* **81**, 507-532 (2012).
3. Bryant, N.J., Govers, R. & James, D.E. Regulated transport of the glucose transporter GLUT4. *Nat Rev Mol Cell Biol* **3**, 267-277 (2002).
4. Fazakerley, D.J., Lawrence, S.P., Lizunov, V.A., Cushman, S.W. & Holman, G.D. A common trafficking route for GLUT4 in cardiomyocytes in response to insulin, contraction and energy-status signalling. *J Cell Sci* **122**, 727-734 (2009).
5. Antonescu, C.N., Diaz, M., Femia, G., Planas, J.V. & Klip, A. Clathrin-dependent and independent endocytosis of glucose transporter 4 (GLUT4) in myoblasts: regulation by mitochondrial uncoupling. *Traffic* **9**, 1173-1190 (2008).
6. Vassilopoulos, S. *et al.* A role for the CHC22 clathrin heavy-chain isoform in human glucose metabolism. *Science* **324**, 1192-1196 (2009).
7. Wakeham, D.E. *et al.* Clathrin heavy and light chain isoforms originated by independent mechanisms of gene duplication during chordate evolution. *Proc Natl Acad Sci U S A* **102**, 7209-7214 (2005).
8. Brodsky, F.M. Diversity of clathrin function: new tricks for an old protein. *Annu Rev Cell Dev Biol* **28**, 309-336 (2012).
9. Liu, S.H. *et al.* A novel clathrin homolog that co-distributes with cytoskeletal components functions in the trans-Golgi network. *EMBO J* **20**, 272-284 (2001).
10. Esk, C., Chen, C.Y., Johannes, L. & Brodsky, F.M. The clathrin heavy chain isoform CHC22 functions in a novel endosomal sorting step. *J Cell Biol* **188**, 131-144 (2010).
11. Jordens, I., Molle, D., Xiong, W., Keller, S.R. & McGraw, T.E. Insulin-regulated aminopeptidase is a key regulator of GLUT4 trafficking by controlling the sorting of GLUT4 from endosomes to specialized insulin-regulated vesicles. *Mol Biol Cell* **21**, 2034-2044 (2010).
12. Dobson, S.P., Livingstone, C., Gould, G.W. & Tavare, J.M. Dynamics of insulin-stimulated translocation of GLUT4 in single living cells visualised using green fluorescent protein. *FEBS Lett* **393**, 179-184 (1996).
13. Dawson, K., Aviles-Hernandez, A., Cushman, S.W. & Malide, D. Insulin-regulated trafficking of dual-labeled glucose transporter 4 in primary rat adipose cells. *Biochem Biophys Res Commun* **287**, 445-454 (2001).
14. Shi, J. & Kandror, K.V. Sortilin is essential and sufficient for the formation of Glut4 storage vesicles in 3T3-L1 adipocytes. *Dev Cell* **9**, 99-108 (2005).
15. Shi, J. & Kandror, K.V. The luminal Vps10p domain of sortilin plays the predominant role in targeting to insulin-responsive Glut4-containing vesicles. *J Biol Chem* **282**, 9008-9016 (2007).
16. Huang, G. *et al.* Insulin responsiveness of glucose transporter 4 in 3T3-L1 cells depends on the presence of sortilin. *Mol Biol Cell* **24**, 3115-3122 (2013).
17. Shewan, A.M. *et al.* GLUT4 recycles via a trans-Golgi network (TGN) subdomain enriched in Syntaxins 6 and 16 but not TGN38: involvement of an acidic targeting motif. *Mol Biol Cell* **14**, 973-986 (2003).

18. Foley, K.P. & Klip, A. Dynamic GLUT4 sorting through a syntaxin-6 compartment in muscle cells is derailed by insulin resistance-causing ceramide. *Biol Open* **3**, 314-325 (2014).
19. Haga, Y., Ishii, K. & Suzuki, T. N-glycosylation is critical for the stability and intracellular trafficking of glucose transporter GLUT4. *J Biol Chem* **286**, 31320-31327 (2011).
20. Trefely, S. *et al.* Kinome Screen Identifies PFKFB3 and Glucose Metabolism as Important Regulators of the Insulin/Insulin-like Growth Factor (IGF)-1 Signaling Pathway. *J Biol Chem* **290**, 25834-25846 (2015).
21. Towler, M.C. *et al.* Clathrin isoform CHC22, a component of neuromuscular and myotendinous junctions, binds sorting nexin 5 and has increased expression during myogenesis and muscle regeneration. *Mol Biol Cell* **15**, 3181-3195 (2004).
22. Martin, S. *et al.* Biogenesis of insulin-responsive GLUT4 vesicles is independent of brefeldin A-sensitive trafficking. *Traffic* **1**, 652-660 (2000).
23. Derre, I. & Isberg, R.R. Legionella pneumophila replication vacuole formation involves rapid recruitment of proteins of the early secretory system. *Infect Immun* **72**, 3048-3053 (2004).
24. Treacy-Abarca, S. & Mukherjee, S. Legionella suppresses the host unfolded protein response via multiple mechanisms. *Nat Commun* **6**, 7887 (2015).
25. Kagan, J.C., Stein, M.P., Pypaert, M. & Roy, C.R. Legionella subvert the functions of Rab1 and Sec22b to create a replicative organelle. *J Exp Med* **199**, 1201-1211 (2004).
26. Watson, R.T. *et al.* Entry of newly synthesized GLUT4 into the insulin-responsive storage compartment is GGA dependent. *EMBO J* **23**, 2059-2070 (2004).
27. Hosaka, T. *et al.* p115 Interacts with the GLUT4 vesicle protein, IRAP, and plays a critical role in insulin-stimulated GLUT4 translocation. *Mol Biol Cell* **16**, 2882-2890 (2005).
28. Tokumitsu, S. & Fishman, W.H. Alkaline phosphatase biosynthesis in the endoplasmic reticulum and its transport through the Golgi apparatus to the plasma membrane: cytochemical evidence. *J Histochem Cytochem* **31**, 647-655 (1983).
29. Li, L.V. & Kandror, K.V. Golgi-localized, gamma-ear-containing, Arf-binding protein adaptors mediate insulin-responsive trafficking of glucose transporter 4 in 3T3-L1 adipocytes. *Mol Endocrinol* **19**, 2145-2153 (2005).
30. Shi, J., Huang, G. & Kandror, K.V. Self-assembly of Glut4 storage vesicles during differentiation of 3T3-L1 adipocytes. *J Biol Chem* **283**, 30311-30321 (2008).
31. Nielsen, M.S. *et al.* The sortilin cytoplasmic tail conveys Golgi-endosome transport and binds the VHS domain of the GGA2 sorting protein. *EMBO J* **20**, 2180-2190 (2001).
32. Kondylis, V. & Rabouille, C. A novel role for dp115 in the organization of tER sites in Drosophila. *J Cell Biol* **162**, 185-198 (2003).
33. Sohda, M. *et al.* The interaction of two tethering factors, p115 and COG complex, is required for Golgi integrity. *Traffic* **8**, 270-284 (2007).
34. Ge, L., Melville, D., Zhang, M. & Schekman, R. The ER-Golgi intermediate compartment is a key membrane source for the LC3 lipidation step of autophagosome biogenesis. *Elife* **2**, e00947 (2013).

35. Hresko, R.C., Murata, H., Marshall, B.A. & Mueckler, M. Discrete structural domains determine differential endoplasmic reticulum to Golgi transit times for glucose transporter isoforms. *J Biol Chem* **269**, 32110-32119 (1994).
36. Hudson, A.W., Ruiz, M. & Birnbaum, M.J. Isoform-specific subcellular targeting of glucose transporters in mouse fibroblasts. *J Cell Biol* **116**, 785-797 (1992).
37. Orme, C.M. & Bogan, J.S. The ubiquitin regulatory X (UBX) domain-containing protein TUG regulates the p97 ATPase and resides at the endoplasmic reticulum-golgi intermediate compartment. *J Biol Chem* **287**, 6679-6692 (2012).
38. Bruno, J., Brumfield, A., Chaudhary, N., Iaea, D. & McGraw, T.E. SEC16A is a RAB10 effector required for insulin-stimulated GLUT4 trafficking in adipocytes. *J Cell Biol* **214**, 61-76 (2016).
39. van Zuylen, W.J. *et al.* Proteomic profiling of the TRAF3 interactome network reveals a new role for the ER-to-Golgi transport compartments in innate immunity. *PLoS Pathog* **8**, e1002747 (2012).
40. Mallard, F. *et al.* Direct pathway from early/recycling endosomes to the Golgi apparatus revealed through the study of shiga toxin B-fragment transport. *J Cell Biol* **143**, 973-990 (1998).
41. Hirst, J., Seaman, M.N., Buschow, S.I. & Robinson, M.S. The role of cargo proteins in GGA recruitment. *Traffic* **8**, 594-604 (2007).
42. Puertollano, R., Aguilar, R.C., Gorshkova, I., Crouch, R.J. & Bonifacino, J.S. Sorting of mannose 6-phosphate receptors mediated by the GGAs. *Science* **292**, 1712-1716 (2001).
43. Atkinson, B.J., Griesel, B.A., King, C.D., Josey, M.A. & Olson, A.L. Moderate GLUT4 overexpression improves insulin sensitivity and fasting triglyceridemia in high-fat diet-fed transgenic mice. *Diabetes* **62**, 2249-2258 (2013).

Figure 1

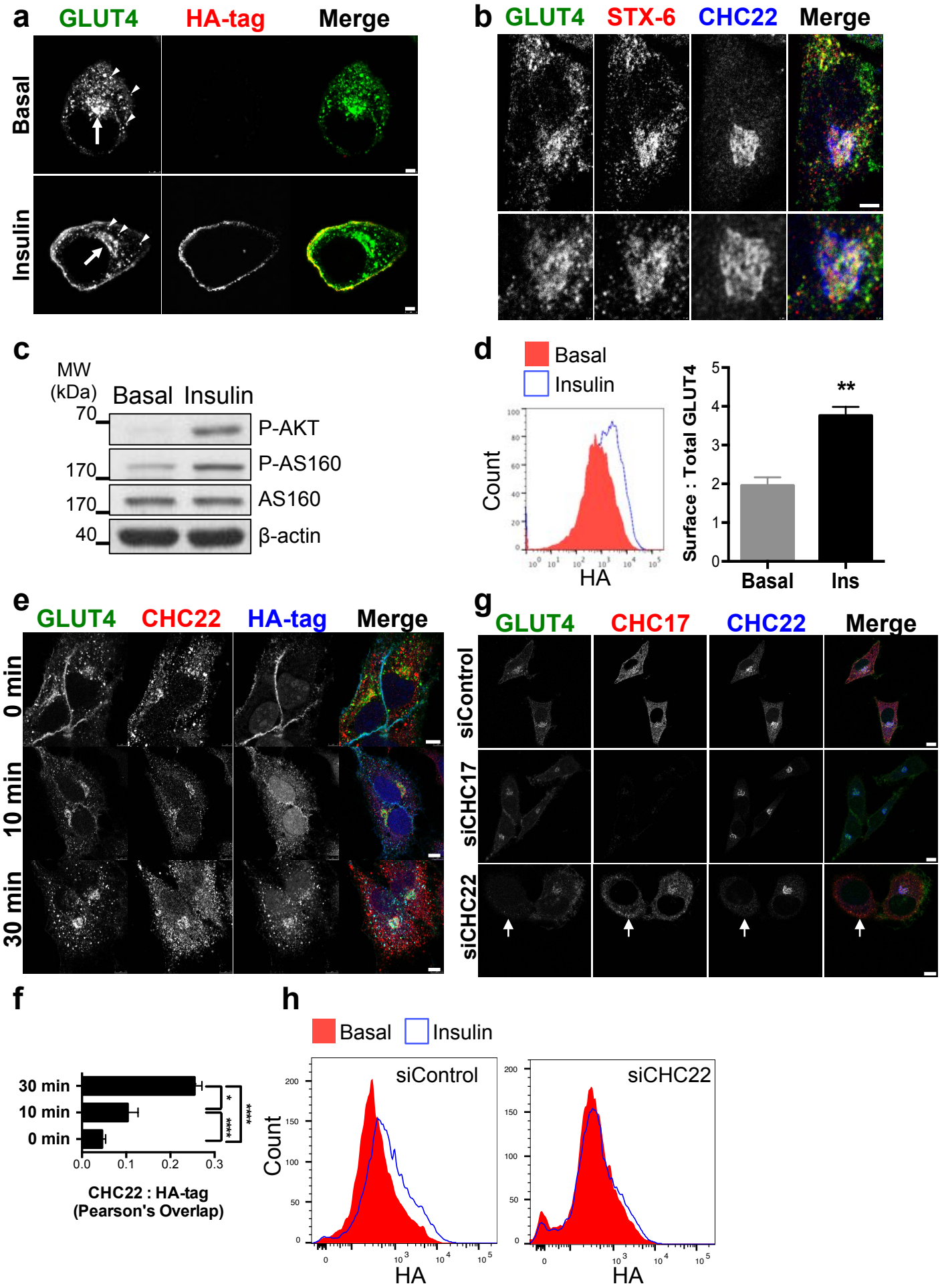
a
GLUT4
HA-tag
Merge
Basal
Insulin
b
GLUT4
STX-6
CHC22
Merge
c
MW (kDa)
Basal
Insulin
70
170
170
40
P-AKT
P-AS160
AS160
β-actin
d
Basal
Insulin
Count
HA
Surface : Total GLUT4
**
Basal
Ins
e
GLUT4
CHC22
HA-tag
Merge
0 min
10 min
30 min
g
GLUT4
CHC17
CHC22
Merge
siControl
siCHC17
siCHC22
f
30 min
10 min
0 min
0.0
0.1
0.2
0.3
*
****
****
CHC22 : HA-tag
(Pearson's Overlap)
h
Basal
Insulin
siControl
siCHC22
Count
HA
HA

Figure 2

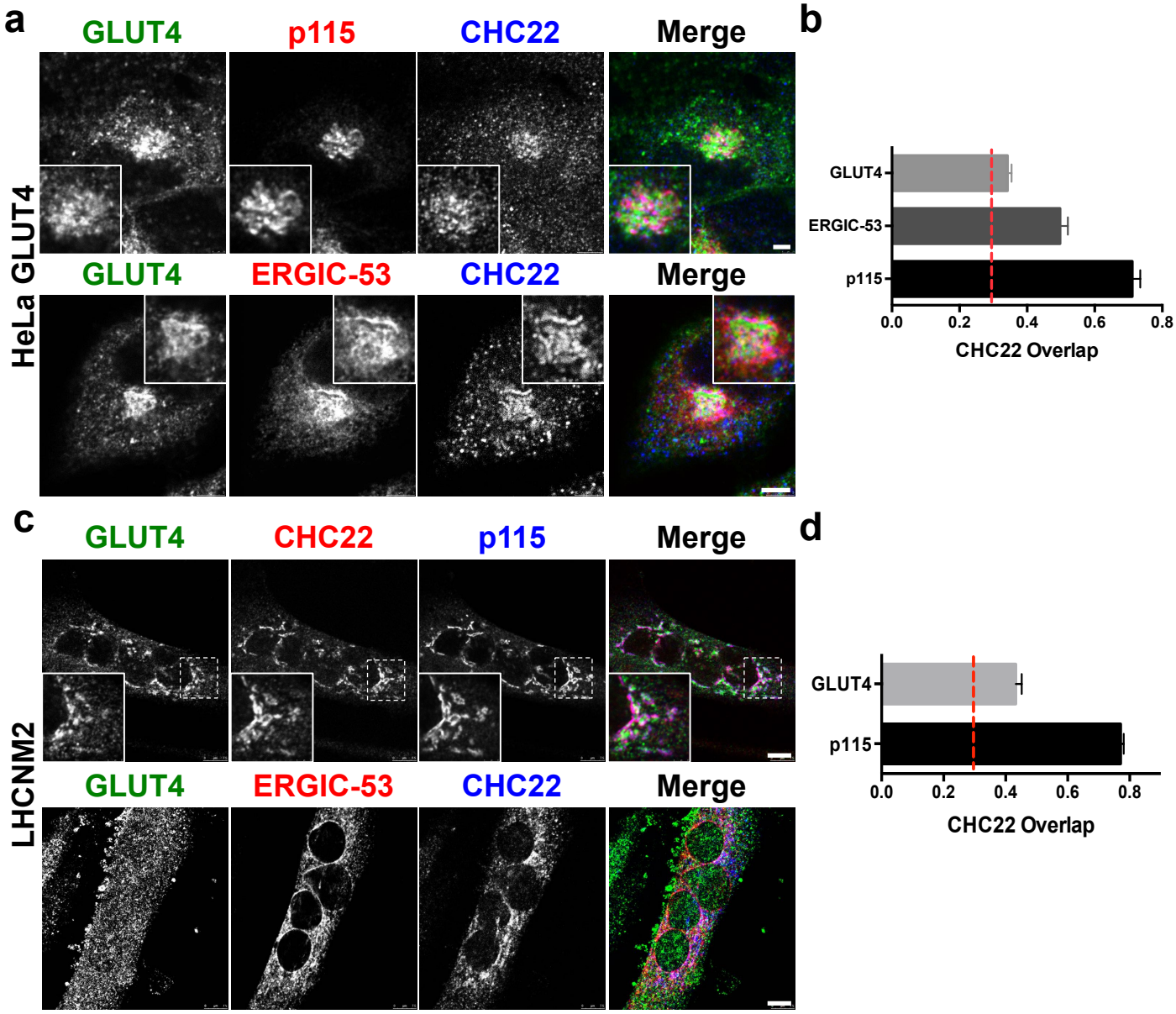
a
GLUT4
p115
CHC22
Merge
HeLa GLUT4
GLUT4
ERGIC-53
CHC22
Merge
b
GLUT4
ERGIC-53
p115
0.0
0.2
0.4
0.6
0.8
CHC22 Overlap
c
GLUT4
CHC22
p115
Merge
LHCNM2
GLUT4
ERGIC-53
CHC22
Merge
d
GLUT4
p115
0.0
0.2
0.4
0.6
0.8
CHC22 Overlap

Figure 3

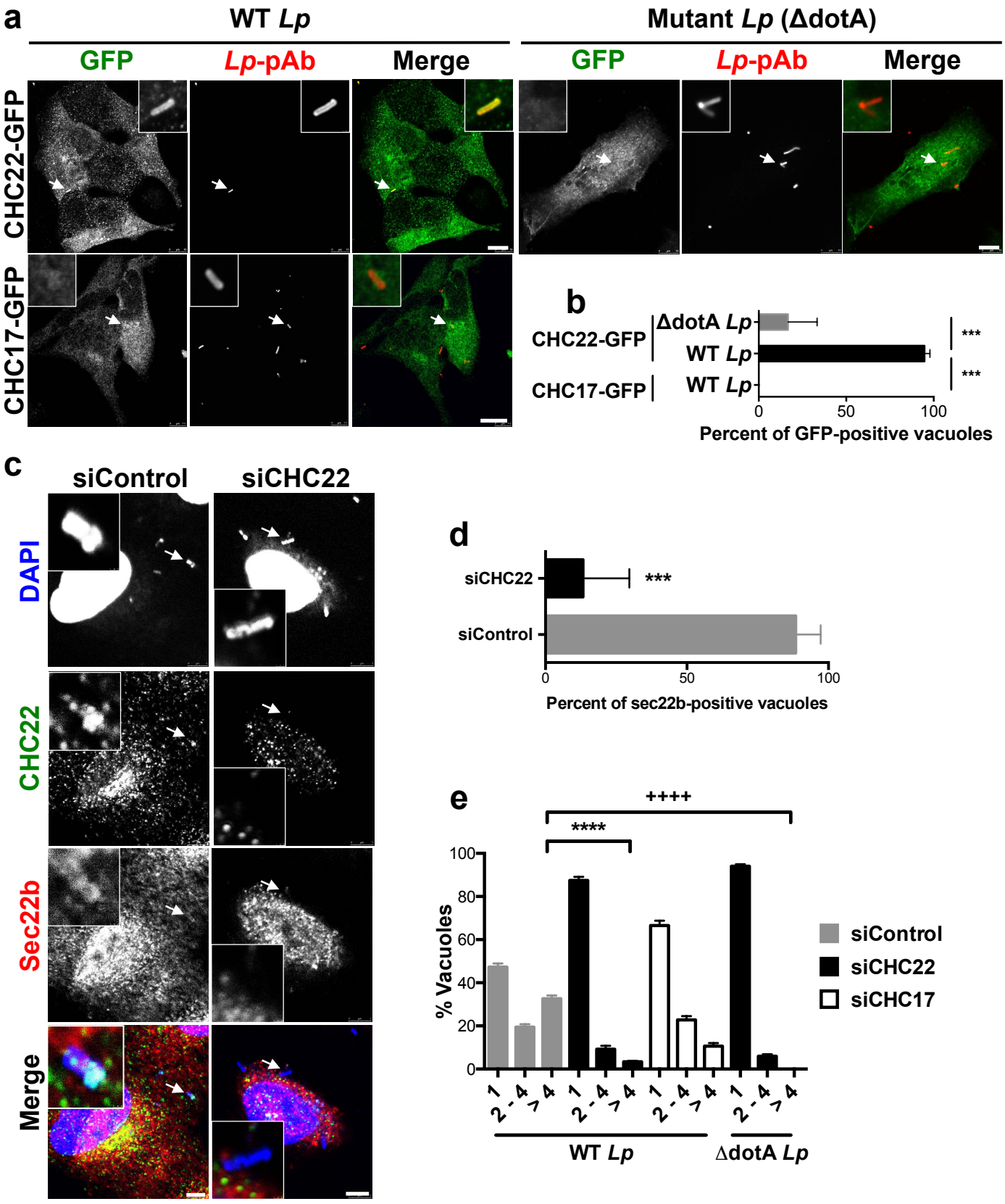
a
WT Lp
Mutant Lp (ΔdotA)
GFP
Lp-pAb
Merge
GFP
Lp-pAb
Merge
CHC22-GFP
CHC17-GFP
b
CHC22-GFP
ΔdotA Lp
WT Lp
CHC17-GFP
WT Lp
***
***
0
50
100
Percent of GFP-positive vacuoles
c
siControl
siCHC22
DAPI
CHC22
Sec22b
Merge
d
siCHC22
siControl
***
0
50
100
Percent of sec22b-positive vacuoles
e
++++
****
100
80
60
40
20
0
% Vacuoles
1
2-4
>4
1
2-4
>4
1
2-4
>4
1
2-4
>4
WT Lp
ΔdotA Lp
siControl
siCHC22
siCHC17

Figure 4

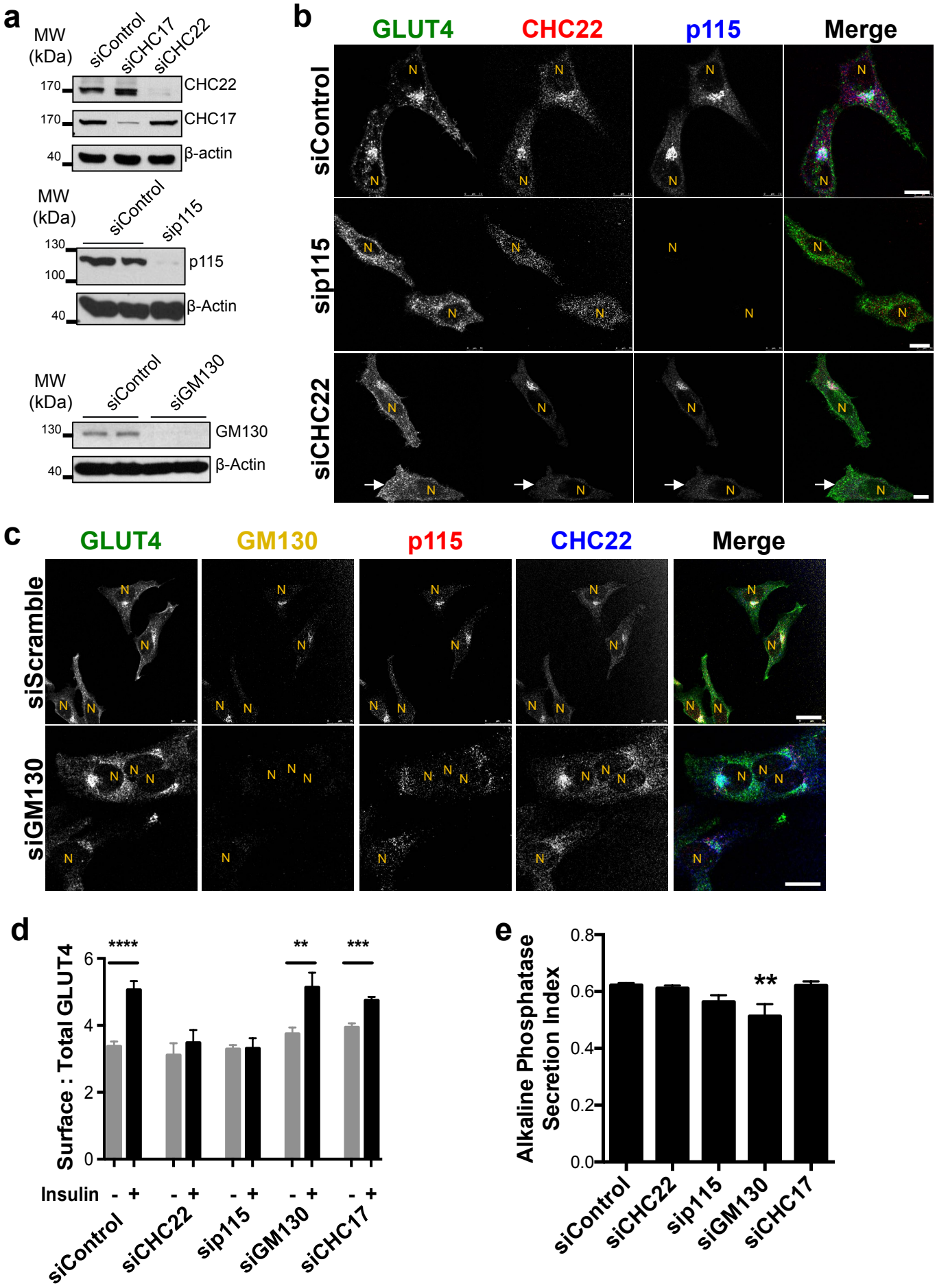
a
MW (kDa)
siControl
siCHC17
siCHC22
170
CHC22
170
CHC17
40
β-actin
MW (kDa)
siControl
sip115
130
100
p115
40
β-Actin
MW (kDa)
siControl
siGM130
130
GM130
40
β-Actin
b
GLUT4
CHC22
p115
Merge
siControl
sip115
siCHC22
N
c
GLUT4
GM130
p115
CHC22
Merge
siScramble
siGM130
N
d
Surface : Total GLUT4
0
2
4
6
****
**
***
Insulin - + - + - + - + - +
siControl
siCHC22
sip115
siGM130
siCHC17
e
Alkaline Phosphatase Secretion Index
0.0
0.2
0.4
0.6
0.8
**
siControl
siCHC22
sip115
siGM130
siCHC17

Figure 5

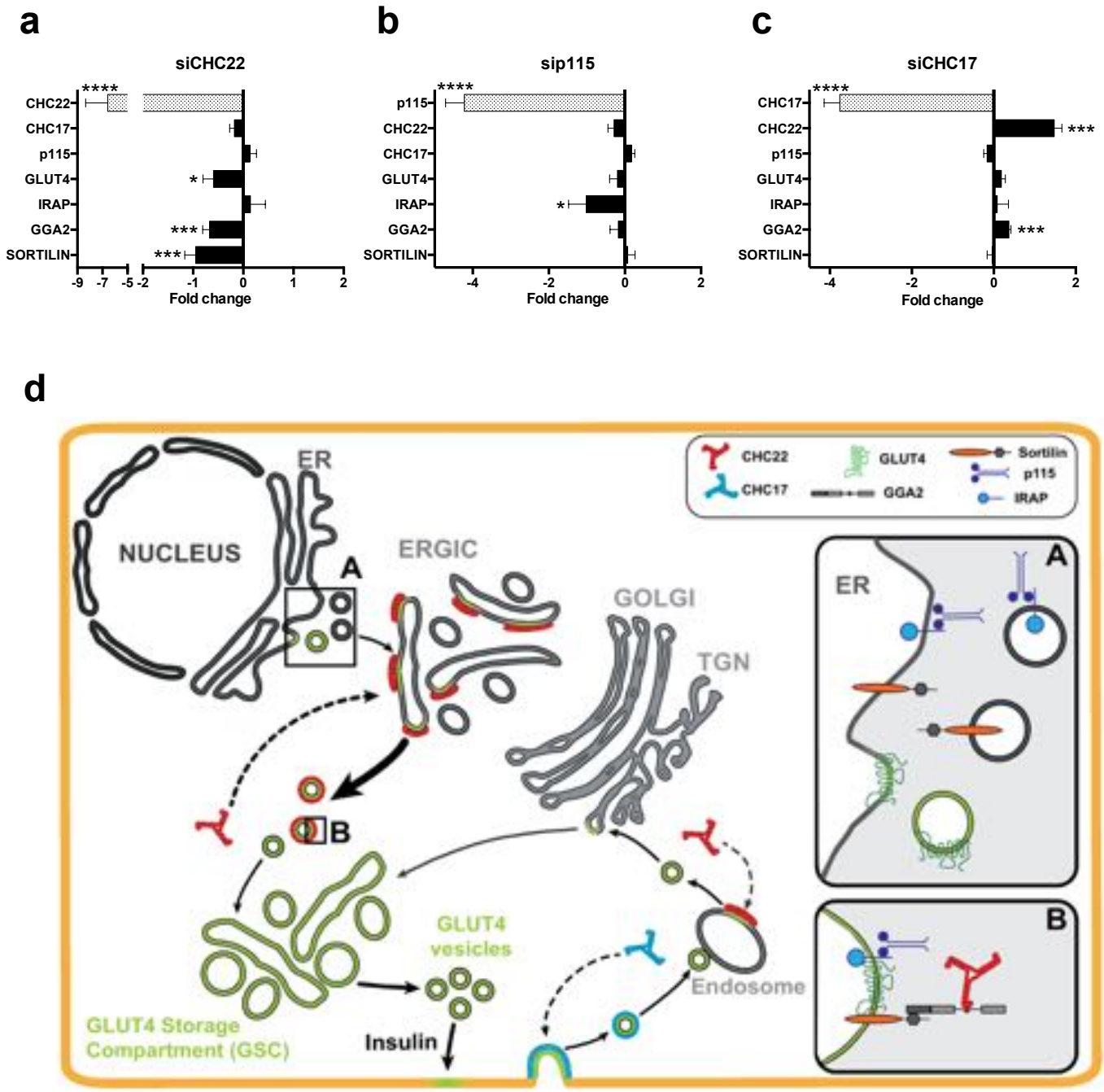
a
siCHC22
CHC22
CHC17
p115
GLUT4
IRAP
GGA2
SORTILIN
****
*
***
***
-9 -7 -5 -2 -1 0 1 2
Fold change
b
sip115
p115
CHC22
CHC17
GLUT4
IRAP
GGA2
SORTILIN
****
*
-4 -2 0 2
Fold change
c
siCHC17
CHC17
CHC22
p115
GLUT4
IRAP
GGA2
SORTILIN
****
***
***
-4 -2 0 2
Fold change
d
NUCLEUS
ER
ERGIC
GOLGI
TGN
A
B
GLUT4 vesicles
Endosome
GLUT4 Storage Compartment (GSC)
Insulin
CHC22
CHC17
GLUT4
GGA2
Sortilin
p115
IRAP
ER
A
B